Three Dimensional Palmprint Recognition using Structured Light Imaging

David Zhang, *Senior Member, IEEE,* Guangming Lu, Wei Li, *Student Member, IEEE,* Lei Zhang, *Member, IEEE,* and Nan Luo

***Abstract*—Palmprint is one of the most unique and stable biometric characteristics. Although 2D palmprint recognition can achieve high accuracy, the 2D palmprint images can be easily counterfeited and much 3D depth information is lost in the imaging process. This paper presents a new approach, 3D palmprint recognition, to exploit the 3D structural information of the palm surface. The structured-light imaging is used to acquire the 3D palmprint data, from which the features of Mean Curvature, Gauss Curvature and Surface Type (ST) are extracted. A fast feature matching and score level fusion strategy are then used to classify the input 3D palmprint data. With the established 3D palmprint database, a series of verification and identification experiments are conducted and the results show that 3D palmprint technique can achieve high recognition rate while having high anti-counterfeiting capability.**

I. Introduction

BIOMETRIC authentication plays an important role in applications of public security, access control, forensic, banking, etc. [1]. The commonly used biometric characteristics include fingerprint, face, iris, signature, gait, etc. In the past decade, palmprint recognition has been growing rapidly [2-4]. However, most of the palmprint recognition techniques are based on the two dimensional (2D) palm images, despite the fact that the human palm is a three dimensional (3D) surface. Although 2D palmprint recognition techniques can achieve high accuracy, the 2D palmprint can be easily counterfeited and much 3D palm structural information is lost. Therefore, it is of high interest to explore new palmprint recognition techniques.

Recently, 3D techniques have been applied to biometric authentication, such as 3D face [5] and 3D ear recognition [6-7]. Range data are usually used in these 3D biometric applications. Most of the existing commercial 3D scanners use laser triangulation to acquire the 3D depth information. Nonetheless, the laser triangulation based 3D imaging technique has some shortcomings for the biometric application. For example, the resolution of 3D cloud point may not be high enough for the accuracy requirement in biometric authentication; if we want to improve the data resolution, the laser scanning speed must be decreased and the requirement of real-time authentication is hard to meet.

With the above considerations, we propose to use structured-light imaging [8-9] to establish the 3D palmprint acquisition system. The structured-light imaging is able to accurately measure the 3D surface of an object but use less time than laser scanning. In the developed system, when the user put his/her palm on the system, a LED projector will generate structured light stripes and project them to the palm. A series of grey level images of the palm with the stripes on it are captured by a CCD camera, and then the depth information of the palm surface is reconstructed from the stripe images.

Compared with other 3D biometric characteristics, 3D palmprint has some desirable properties. For instance, it is more convenient to collect and more user friendly; projecting stripes on palm has much higher acceptability than on face. One disadvantage of 3D palmprint may be that the palm surface is relatively plane so that the depth information of palm is more difficult to capture than that of face or ear. However, as can be seen in this paper, with the proposed feature extraction and matching procedures, the 3D palmprint recognition can reach very high accuracy.

In this paper, we will extract the local curvature features of 3D palmprint for classification and matching. After the 3D depth information of palm is obtained, a sub-area, call the Region of Interest (ROI), is extracted. The Mean curvature and Gaussian curvature features of each cloud point in the ROI are then calculated. To save storage space and speed up the matching process, we convert the curvature features to grey level images, i.e. the Mean Curvature Image (MCI) and Gaussian Curvature Images (GCI). Another type of 3D feature, the Surface Types (ST) of the palmprint is also extracted. Finally, the input palm is classified and recognized using the MCI/GCI and ST features. A 3D palmprint database with 6000 samples from 260 people is established and a series of experiments are conducted to evaluate the performance of the proposed scheme.

The rest of the paper is organized as follows. Section II describes the acquisition of 3D palmprint data. Section III discusses the ROI region determination, the 3D feature extraction and the feature matching method. Section IV presents the experimental results and Section V concludes the paper.

David Zhang, Lei Zhang, and Nan Luo are with the Department of Computing, Hong Kong Polytechnic University, Hong Kong, China. (e-mail: csdzhang@comp.polyu.edu.hk, cslzhang@comp.polyu.edu.hk).

Wei Li is with the Institute of Image Processing and Pattern Recognition, Shanghai Jiao Tong University, Shanghai, China. (e-mail: liweistorm@sjtu.edu.cn).

Guangming Lu is with Shenzhen Graduate School, Harbin Institute Technology, Shenzhen, China. (e-mail: luguangm@gmail.com).

978-1-4244-2730-7/08/$25.00 ©2008 IEEE

II. 3D PALMPRINT DATA ACQUISITION

The commonly used 3D imaging techniques include multi-viewpoint reconstruction [11], laser scanning [12] and structured light scanning [8]. Structured-light scanning can measure the object surface in a high accuracy and in a relatively short time period. Considering the requirements of accuracy and speed in biometric authentication, we choose to use structured light scanning to acquire the palm depth information.

The using of structured light in object surface measurement can be tracked back to 2 decades ago [8]. Since then, it has been widely used in 3D object measurement, 3D shape reconstruction, reverse engineering, etc [13-15]. In structured light imaging, a light source projects some structured light patterns (stripes) onto the surface of the object. The reflected light is captured by a CCD camera and then a series of images are collected. After some calculation, the 3D surface depth information of the object can be obtained.

In our developed system, a cost-effective grey LCD projector with LED light source is employed, and some shift light patterns are projected onto the palm. For more details about structured light imaging, please refer to [8]. With the phase shifting and unwrapping techniques [9], we can retrieve the depth information of the object surface by projecting a series of different phase stripes on it. The range data of the palm surface can then be obtained. In our system, the spatial resolution of the 3D image is set as 768×576. Some sample patterns of the stripes on the palm are illustrated in Fig. 1, and an example 3D palmprint image is shown in Fig. 2.

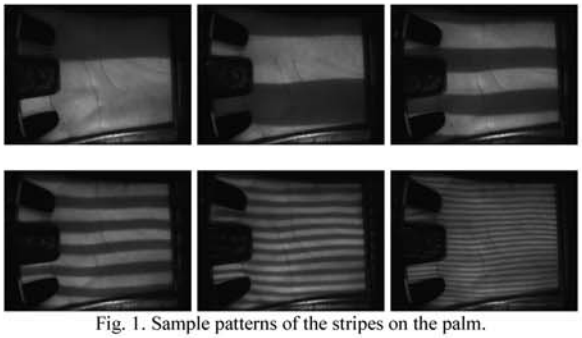

Fig. 1. Sample patterns of the stripes on the palm.

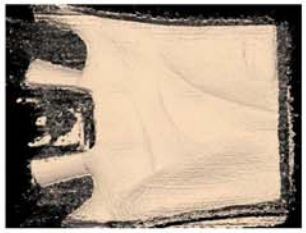

Fig. 2. An example 3D palmprint image.

III. FEATURE EXTRACTION FROM 3D PALMPRINT

A. ROI Extraction

From Fig. 2, we can see that in the 3D palmprint image of resolution 768×576, many cloud points, such as those in the boundary area and those in the fingers, could not be used in the feature extraction and recognition. Most of the useful and stable features locate in the center area of the palm. On the other hand, in different times the user puts his/her palm on the system, there will be some relative displacements of the positions of the palm, even when we impose some constraints on the users to place their hand. Therefore, before feature extraction it is necessary to perform some preprocessing to align the palmprint and extract its central area, which is called the Region of Interest (ROI).

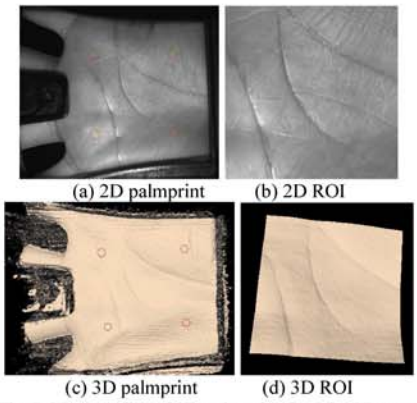

(a) 2D palmprint (b) 2D ROI

(c) 3D palmprint (d) 3D ROI

Fig. 3. The ROI extraction of 3D palmprint from its 2D counterpart.

In the 3D palmprint acquisition process, we can simultaneously capture a 2D palmprint image. The algorithm in [3] can be performed to extract the 2D ROI, which is then mapped to 3D data for the 3D ROI. Fig. 3 illustrates the ROI extraction process. After the 2D ROI is obtained, the 3D ROI is extracted by preserving the 3D points in the positions indicated by the 2D ROI.

With ROI extraction, the 3D palmprints are aligned and normalized. The small translation and rotation introduced in the data acquisition process are then corrected. In addition, the data amount used in the following feature extraction and matching process is significantly reduced. This will save much computational cost.

B. Curvature Calculation

The depth information in the acquired 3D palmprint reflects the relative distance between the reference plane and each point in the object. The z-values of the 3D cloud points are affected by the position of hand in scanning. However, each time the users put their hands, the 3D space locations will be different. The ROI extraction process can only correct, to some extent, the rotation and translation displacements in the x-y plane but not the z-axis. In addition, the human palm is not a rigid object and it can have some deformation. Those factors introduce much noise in the 3D palmprint cloud points and make the well-known ICP algorithms [10] not suitable for 3D palmprint recognition. Instead, the local invariant features, such as the curvatures [18] of a surface, will be much more stable in representing the characteristics of 3D palmprint.

Let p be a point on the surface S. Consider all curves C_i on S passing through the point p on the surface. Each curve C_i will have an associated curvature K_i at p. Among those curvatures K_i, at least one is characterized as maximal k_1 and one as minimal k_2, and these two curvatures k_1 and k_2 are known as the principal curvatures of point p on the surface [18]. The Mean curvature H and the Gaussian curvature K of p are defined as follows

$$H = (k_1 + k_2)/2 \text{ and } K = k_1 * k_2 \quad (1)$$

The Mean and Gaussian curvatures are intrinsic measures of a surface, i.e. they depend only on the surface shape but not on the way how the surface is placed in the 3D space [18]. Thus such curvature features are robust to the rotation, translation and even some deformation of the palm. The captured 3D palmprint data are organized range data. We adopt the algorithm in [19] to estimate the Mean and Gaussian curvatures for its simplicity and effectiveness.

Given an input 3D palmprint image I, we first use a 7×7 mean filter F to smooth it

$$\tilde{I} = F * I \quad (2)$$

where symbol "*" denotes 2D convolution.

Then, five 7×7 templates D_u, D_v, D_{uu}, D_{vv} and D_{uv} are defined to estimate the partial derivatives of filtered images $\tilde{I}$. The five templates are spanned using three vectors $\vec{d}_0$, $\vec{d}_1$ and $\vec{d}_2$ as follows [19]

$$D_u = \vec{d}_0 \times \vec{d}_1^T,\ D_v = \vec{d}_1 \times \vec{d}_0^T,\ D_{uu} = \vec{d}_0 \times \vec{d}_2^T,$$
$$D_{vv} = \vec{d}_2 \times \vec{d}_0^T,\ D_{uv} = \vec{d}_1 \times \vec{d}_1^T \quad (3)$$

The three vectors are set as $\vec{d}_0 = [1,1,1,1,1,1,1]^T/7$, $\vec{d}_1 = [-3,-2,-1,0,1,2,3]^T/28$, $\vec{d}_2 = [5,0,-3,-4,-3,0,5]^T/84$.

The five templates are then convoluted with $\tilde{I}$ to get the derivative images of $\tilde{I}$:

$$\tilde{I}_t = D_t * \tilde{I},\ t \in \{u, v, uu, vv, uv\} \quad (4)$$

With the five derivative images $\tilde{I}_t$, the Mean (H) and Gaussian (K) curvatures are computed as:

$$H(i,j) = \frac{H_1(i,j) + H_2(i,j) - 2H_3(i,j)}{2(\sqrt{1 + \tilde{I}_u^2(i,j) + \tilde{I}_v^2(i,j)})^3} \quad (5)$$

$$K(i,j) = \frac{\tilde{I}_{uu}(i,j)\tilde{I}_{vv}(i,j) - \tilde{I}_{uv}^2(i,j)}{(1 + \tilde{I}_u^2(i,j) + \tilde{I}_v^2(i,j))^2} \quad (6)$$

where $H_1(i,j) = (1 + \tilde{I}_v^2(i,j))\tilde{I}_{uu}(i,j)$, $H_2(i,j) = (1 + \tilde{I}_u^2(i,j))\tilde{I}_{vv}(i,j)$ and $H_3(i,j) = \tilde{I}_u(i,j)\tilde{I}_v(i,j)\tilde{I}_{uv}(i,j)$.

C. Mean Curvature Image (MCI) and Gaussian Curvature Image (GCI)

With equations (5) and (6), the Mean and Gaussian curvatures of a 3D palmprint image can be calculated. For better visualization and more efficient computation, we convert the original curvature images into grey level images with integer pixels. We first transform the curvature image C (Gaussian curvature K or Mean curvature H) to $\bar{C}$ as follows

$$\bar{C}(i,j) = 0.5(C(i,j) - \mu)/(4\delta) + 0.5 \quad (7)$$

where μ is the mean of the curvature image. With (7), most of the curvature values will be normalized into the interval [0,1]. We then map $\bar{C}(i,j)$ to an 8-bits grey level image $G(i,j)$:

$$G(i,j) = \begin{cases} 0 & \bar{C}(i,j) \le 0 \\ round\left(255 \times \bar{C}(i,j)\right) & 0 < \bar{C}(i,j) < 1 \\ 255 & \bar{C}(i,j) \ge 1 \end{cases} \quad (8)$$

We call the images $G(i,j)$ the Mean Curvature Image (MCI) and Gaussian Curvature Image (GCI), respectively for Mean and Gaussian curvatures. Fig. 4 illustrates the MCI and GCI images of two different palms and Fig. 5 illustrates the MCI and GCI images of the same palm at two different acquisition times.

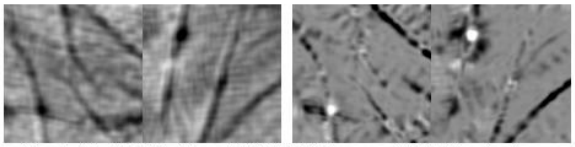

Fig. 4. The MCI (left) and GCI (right) images of 2 different palms.

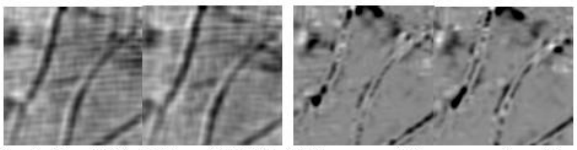

Fig. 5. The MCI (left) and GCI (right) images of the same palm at two different times.

From Figs. 4 and 5, we can see that the MCI and GCI images can well preserve and reflect the 3D palm surface features. Not only the principle lines, which are the most important texture features in both 2D and 3D palmprint recognition, are clearly enhanced in MCI/GCI, but also the depth information of different shape structures is well preserved. The MCI/GCI feature images provide us a good basis for further processing and pattern matching.

D. Points Classification using Surface Types (ST)

TABLE I
SURFACE TYPE LABELS FROM CURVATURE SIGNS

	$K > 0$	$K = 0$	$K < 0$
$H < 0$	Peak, ST=1	Ridge, ST=2	Saddle Ridge, ST=3
$H = 0$	None, ST=4	Flat, ST=5	Minimal Surface, ST=6
$H > 0$	Pit, ST=7	Valley, ST=8	Saddle Valley, ST=9

The palm is a continuous surface with different convex and concave structures. Besides MCI/GCI features, we can also classify the points in the palm into different groups based on their local surface characteristics. Such kind of 3D feature is

called Surface Type (ST), which can be determined from the signs of Mean and Gaussian curvature values. In [19], eight fundamental surface types (ST) were defined based on the Mean and Gaussian curvatures. Table I lists the definition of the ST types.

From Table I we see that the STs are defined according to the different combinations of the signs of Mean and Gaussian curvatures. Therefore, in total nine STs can be defined, including eight fundamental STs and one special case for H=0 and K>0. Using STs, the points in the 3D palmprints can be intuitively classified into nine classes. However, the values in curvature matrices H and K are floating-point numbers. We need to quantize them to fix the intervals that make H=0 and K =0. This can be simply implemented by using two thresholds ε_H and ε_K:

$$\begin{cases} H(i,j)=0 & if \quad |H(i,j)|<\varepsilon_H \\ K(i,j)=0 & if \quad |K(i,j)|<\varepsilon_K \end{cases} \tag{9}$$

The only problem in (9) is that the thresholds ε_H and ε_K should be adaptive to different palms. To this end, we first normalize the Mean or Gaussian curvature $C(i,j)$ by its standard deviation as

$$C_s(i,j)=C(i,j)/2\delta \tag{10}$$

Using (10), most curvature values will fall into the interval [-1,1] without changing their sign. Then, we can easily set the thresholds ε_H and ε_K around zero for C_s.

With the above procedures, each point in the 3D palmprint can be classified into one of the nine surface types. Fig. 6 shows the point classification results of a palm sample using binary images.

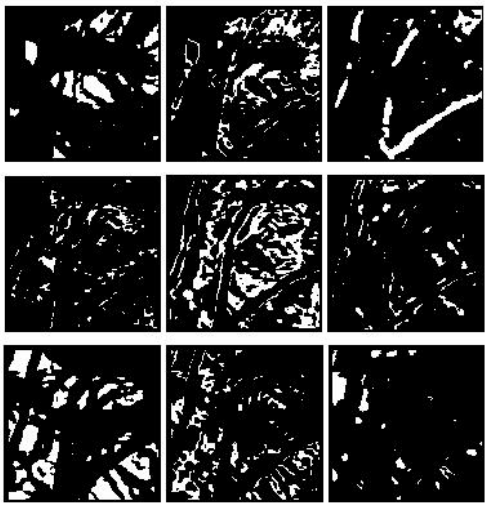

Fig. 6. From left to right, top to bottom: surface types 1 to 9 of a palm.

E. Feature Matching and Fusion

Now we have the MCI, GCI and ST features of the 3D palmprint. The different palmprints can then be matched. In this section, we discuss the matching strategy of different features and the score level fusion of them.

MCI/GCI Feature Matching. The MCI/GCI features are 8-bits grey level images. To reduce the computational cost and improve the speed of feature matching, here we transform the MCI/GCI into binary images using adaptive thresholding:

$$B(i,j)=\begin{cases} 1 & G(i,j)<c\cdot\mu_G \\ 0 & others \end{cases} \tag{11}$$

where c is a constant and μ_G is the mean value of $G(i,j)$. Based on our experimental experience, we set c = 0.7 in the experiments.

We use the AND operation to calculate the matching score of MCI/GCI features. Denote by B_d the binarized MCI/GCI image in the database and by B_t the input MCI/GCI binary image. Suppose the image size is n×m. The matching score between B_d and B_t is defined as:

$$R_C=\frac{2\sum_{i=1}^{n}\sum_{j=1}^{m}B_d(i,j)\oplus B_t(i,j)}{\sum_{i=1}^{n}\sum_{j=1}^{m}B_d(i,j)+\sum_{i=1}^{n}\sum_{j=1}^{m}B_t(i,j)} \tag{12}$$

where symbol "⊕" means the AND logic operation. If the two MCI/GCI binary feature images B_d and B_t are identical, we then have R_c=1; the minimum value of R_c is 0, which means that the two binary images have no overlap "1" pixel.

Since there may still have some displacements between the two palmprint images even after ROI extraction, when calculating the matching score by (12), we will shift one pixel of the test image along 8 directions: right, left, up, down, left-up, left-down, right-up and right-down. Thus we will have 9 matching scores and the maximum one is selected.

ST Feature Matching. For each 3D palmprint, we have 9 binary ST images, representing different surface types of the points in it. Denote by ST_k^d, k=1,2,…,9, the ST images in database and by ST_k^t the test ST images. Different from the matching score of MCI/GCI features, here we use the absolute value of difference (AVD) to measure the distance between two palmprints:

$$R_{ST}=1-\frac{\sum_{k=1}^{9}\sum_{i=1}^{n}\sum_{j=1}^{m}\left|ST_k^d(i,j)-ST_k^t(i,j)\right|}{2\times m\times n} \tag{13}$$

If the ST features of two palmprints are identical, we have the maximum matching score R_{ST}=1; on the contrary, if the ST features are extremely different, the ST matching score will be R_{ST}=0.

Matching Score Fusion. Using equations (12) and (13), three matching scores (two R_c scores for MCI and GCI respectively, and one R_{ST} score for ST) can be calculated. Each one of them can be used to make a decision and the three

decisions can be fused for the final decision. Another way is to fuse the three matching scores first and then make the decision based on the fused matching score. Here we adopt the second strategy.

Suppose there are n matching scores and denote them by R_i, i=1,2,…,n. Many score level fusion techniques can be used, such as Min-Score, Max-Score, Average and Weighted Average methods [20]. Here we use the Weighted Average method. As mentioned in section III, the Mean curvature contains more useful information than Gaussian curvature so that the MCI feature can lead to better result than GCI (referring to section IV please). We should assign a higher weight to MCI than GCI. Because the EER (Equal Error Rate) values are indicators of the discriminability of the associated features and they can be estimated by the test database, we set the weights of the feature matching scores based on their EER values. This fusion method is called Matcher Weighting [20], which is defined as

$$R_f = \sum_{i=1}^{n} w_i R_i \quad , \quad w_i = \frac{1}{e_i} \Big/ \sum_{j=1}^{n} \frac{1}{e_j} \tag{14}$$

where w_i is the weight of R_i and e_i is the corresponding EER.

IV. Experimental Results

A. Anti- counterfeiting Test

One clear advantage of 3D palmprint recognition over 2D palmprint is that it has higher anti-counterfeiting capability because a 3D palm is much harder to forge. In this section we made a simple anti-counterfeiting test by using a printed 2D palm image. A user is registered in both the 2D palmprint and 3D palmprint systems. We printed out a 2D palmprint image of this user on a piece of paper using a high quality laser printer (HP LaserJet 1020plus, 1200dpi). Then we put this paper on the two systems as input palm to see if it can pass the systems.

Figs. 7 and 8 illustrate the two tests and the recognition results. In Fig. 7 we can see that because the printed palm is a pure paper plane and the real palm is a curved surface, the captured palmprint images from printed palm and real palm will have some differences on illumination level. However, the features (principle lines, wrinkles, etc) of the two images are very similar and the system will successfully match the printed palm with the palmprint in the database because the 2D palmprint recognition algorithms [3] are robust to illumination variations to some extent.

As what we expected, in Fig. 8 it can be seen that 3D palmprint technique can easily tell the counterfeited palm because there is no depth information in the printed paper and the captured 3D palmprint image from the printed 2D palmprint is just a noise image. Of course, people can also forge a 3D palm but this will be much more difficult and require much more cost than forging the 2D palm.

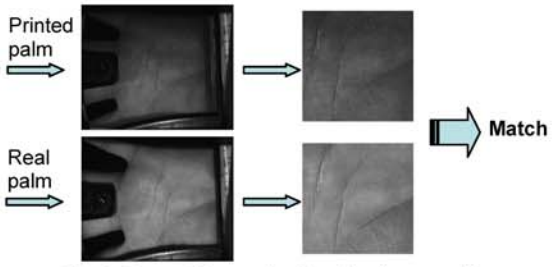

Fig. 7. Counterfeit test using 2D palmprint recognition.

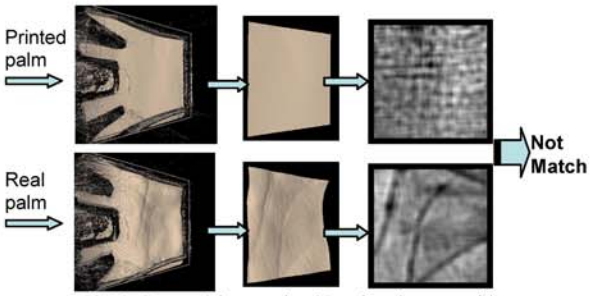

Fig. 8. Counterfeit test using 3D palmprint recognition.

B. Database and Recognition Results

A 3D palmprint database was established by using the developed 3D palmprint imaging device. The database contains 6000 samples from 260 volunteers, including 182 males and 78 females. The 3D palmprint samples were collected in two separated sessions, and in each session, about 12 samples were collected from a person. The average time interval between the two sessions is two weeks. The original spatial resolution of the data is 768×576. After ROI extraction, the central part (256 ×256) is used for feature extraction and recognition. The z-value resolution of the data is 32 bits.

We performed two types of experiments on the established database: verification and identification. In verification, the class of the input palmprint is known and each of the 3D samples was matched with all of the other 3D samples in the database. A successful matching is called intra-class matching or genuine if the two samples are from the same class. Otherwise, the unsuccessful matching is called inter-class matching or impostor. Using the established database, there are 17,997,000 matching in total. The verification experiments were performed by using each of the MCI, GCI and ST features, as well as the combination of them using the score level fusion (referring to (14) please). The ROC curves are shown in Fig. 9. The EER values are listed in Table II, where the feature extraction and matching time by using different features are also listed[1].

The experiments of identification were also conducted on the 3D palmprint database. In identification, we do not know the class of the input palmprint but want to identify which class it belongs to. In the experiments we let the first sample of

[1] The experiments were performed using Visual C++ 6.0 on a PC with Windows XP Professional, Pentium 4 CPU of 2.66GHz and 1GB RAM.

each class in the database be template and use the other samples as probes. Therefore, there are 5480 probes and 520 templates. The probes were matched with all the templates models, and they were assigned to the class that yields the highest matching score. The identification results are listed in Table III.

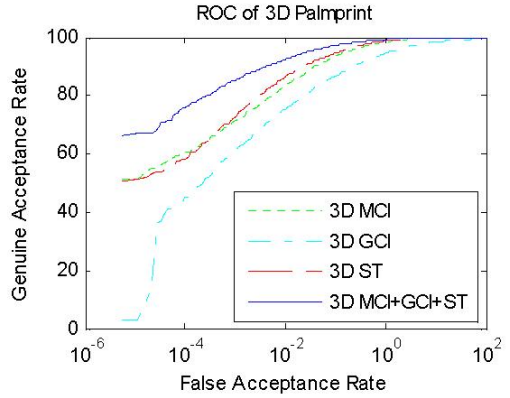

Fig. 9. Comparison of ROC of 3D methods.

TABLE II
VERIFICATION EER, FEATURE EXTRACTION TIME AND MATCHING TIME BY DIFFERENT TYPES OF FEATURES.

	MCI	GCI	ST	MCI+GCI+ST
EER (verification)	1.25%	3.13%	1.13%	0.81%
Feature extraction time	112ms	112ms	115ms	125ms
Matching time	0.86ms	0.86ms	3.76ms	4.89ms

TABLE III
THE IDENTIFICATION ACCURACY BY DIFFERENT TYPES OF FEATURES.

	MCI	GCI	ST	MCI+GCI+ST
Identification accuracy	98.48%	95.69%	98.30%	98.92%

V. CONCLUSIONS

In this paper, we explored a new technique for palmprint based biometrics: 3D palmprint recognition. First a structured light based 3D palmprint data acquisition system was developed. After the 3D palmprint image is captured, the region of interest (ROI) is extracted to roughly align the palm and remove the unnecessary cloud points. We then developed the curvature based feature extraction algorithms to obtain the Mean Curvature Image (MCI), Gaussian Curvature Image (GCI) and Surface Type (ST) features. A fast feature matching method and a score level feature fusion strategy were used to classify the palmprints. A 3D palmprint database with 6000 samples from 260 individuals was established, on which a series of verification and identification experiments were performed. The experimental results show that 3D palmprint technique can not only achieve very high recognition rate but also have high anti-counterfeit capability. In the future, more advanced and powerful feature extraction and matching techniques are to be developed for a better recognition performance.

ACKNOWLEDGMENT

This work is supported by the ITF Guangdong-Hong Kong Technology Cooperation Funding Scheme under grant no. ZP5C.

REFERENCES

[1] R.M. Bolle, J.H. Connell, S. Pankanti, N.K. Ratha, and A.W. Senior, *Guide to Biometrics*, Springer, U.S., 2003.

[2] W. Shu and D. Zhang, "Automated personal identification by palmprint", Optical Engineering, vol. 38, no. 8, pp. 2359-2362, 1998.

[3] D. Zhang, A.W.K. Kong, J. You, and M. Wong, "On-line palmprint identification," *IEEE Transactions on Pattern Analysis and Machine Intelligence,* vol. 25, no. 9, pp. 1041-1050, 2003.

[4] A.W.K. Kong and D. Zhang, "Competitive coding scheme for palmprint verification," *Proceedings of International Conference on Pattern Recognition,* vol. 1, pp. 520-523, 2004.

[5] C. Samir, A. Srivastava, and M. Daoudi, "Three-dimensional face recognition using shapes of facial curves," *IEEE Transactions on Pattern Analysis and Machine Intelligence,* vol. 28, no. 11, pp. 1858 - 1863, Nov. 2006.

[6] H. Chen and B. Bhanu, "Human ear recognition in 3D," *IEEE Transactions on Pattern Analysis and Machine Intelligence,* vol. 29, no. 4, pp. 718-737, April 2007.

[7] P. Yan and K. W. Bowyer, "Biometric recognition using 3D ear shape", *IEEE Transactions on Pattern Analysis and Machine Intelligence,* vol. 29, no. 8, pp. 1297-1308, Aug. 2007.

[8] V. Srinivassan and H.C. Liu, "Automated phase measuring profilometry of 3D diffuse object," *Appl. Opt.,* 23(18): 3105-3108, 1984.

[9] H.O. Saldner and J.M. Huntley, "Temporal phase unwrapping: application to surface profiling of discontinuous objects," *Appl.Opt.,* 36(13):2770-2775, 1997.

[10] P. J. Besl and N.D. McKay, "A method for registration of 3-D shapes," *IEEE Transactions on Pattern Analysis and Machine Intelligence,* vol. 14, no. 2, pp. 239 - 256, Feb. 1992.

[11] R. Hartley, *Multiple View Geometry in Computer Vision,* Cambridge, New York: Cambridge University Press, 2000.

[12] F. Blais, M. Rious, and J.A. Beraldin, "Practical considerations for a design of a high precision 3-D laser scanner system," *Proc. SPIE,* vol. 959, pp. 225-246, 1988.

[13] S.M. Dunn, R.L. Keizer, and J. Yu, "Measuring the area and volume of the human body with structured light," *IEEE Transactions on Systems, Man and Cybernetics,* vol. 19, no. 6, pp. 1350- 1364, Nov.-Dec. 1989.

[14] G. Hu and G. Stockman, "3-D surface solution using structured light and constraint propagation," *IEEE Transactions on Pattern Analysis and Machine Intelligence,* vol. 11, no. 4, pp. 390 – 402, April 1989.

[15] A.C. Sanderson, L.E. Weiss, and S.K. Nayar, "Structured highlight inspection of specular surfaces," *IEEE Transactions on Pattern Analysis and Machine Intelligence,* vol. 10, no. 1, pp. 44-55, Jan. 1988.

[16] G. C. Stockman, S.W. Chen, G. Hu, and N. Shrikhande, "Sensing and recognition of rigid objects using structured light," *Control Systems Magazine, IEEE,* vol. 8, no. 3, pp. 14-22, June 1988.

[17] G. Sansoni, L. Biancardi, U. Minoni, and F. Docchio, "A novel, adaptive system for 3-D optical profilometry using a liquid crystal light projector," *IEEE Transactions on Instrumentation and Measurement,* vol. 43, no. 4, pp. 558-566, Aug. 1994.

[18] W. Kühnel, *Differential Geometry: Curves-Surfaces-Manifolds,* American Mathematical Society, 2006.

[19] P.J. Besl and R.C. Jain, "Segmentation through variable-order surface fitting," *IEEE Transactions on Pattern Analysis and Machine Intelligence,* vol. 10, no. 2, pp. 167 - 192, March 1988.

[20] R. Snelick, U. Uludag, A. Mink, M. Indovina, and A. Jain, "Large-scale evaluation of multimodal biometric authentication using state-of-the-art systems," *IEEE Transactions on Pattern Analysis and Machine Intelligence,* vol. 27, no. 3, pp. 450- 455, March 2005.